VI.5. ACTIVATION AND CHARACTERIZATION STUDIES OF COMMERCIAL FISCHER-TROPSCH IRON CATALYSTS (Robert J. O'Brien, Liguang Xu, Robert L. Spicer, Diane R. Milburn and Burtron H. Davis, K. R. P. M. Rao, Frank E. Huggins and G. P. Huffman)

VI.5.1. INTRODUCTION

Much of the effort at the CAER has been focused on the testing of catalysts prepared by United Catalysts Inc. These catalysts have been screened as possible candidates to be used in the slurry-bubble column reactor operated by Air Products, Inc at La Porte, Texas. A critical factor in the activity and selectivity of iron catalysts is the method of activation (VI.5.1). Kölbel used CO rich synthesis gas at a temperature of 15-30°C above the synthesis temperature to activate a doubly promoted iron catalyst used in the Rheinpreussen-Koppers demonstration plant (VI.5.2). Bukur et al. have demonstrated that CO activation results in better overall activity and selectivity than activation in H_2 or synthesis gas (VI.5.3). Huang et al. have shown that an ultrafine ferric oxide catalyst has twice the activity when pretreated in CO than when pretreated in H_2 (VI.5.4,VI.5.5).

In the present study, industrially prepared iron oxide catalysts promoted with potassium and copper have been studied in the slurry phase using continuous stirred tank reactors (Table VI.5.1). Activations in synthesis gas, similar to that used by Kölbel, were studied as was activation in CO (Table VI.5.2). Catalysts samples taken at various times during the pretreatment and synthesis were characterized by XRD, Mössbauer spectroscopy, BET analysis and elemental analysis and the results were correlated with catalyst activity and selectivity.

VI.5.2. EXPERIMENTAL

RJO043 - 19.0 g of UCI L-3950 catalyst and 76 g of C30 oil were added to a 300 mL autoclave. Synthesis gas was started ($H_2/CO=0.7$) at a space velocity of 2.0 nL/hr/g(Fe) and a pressure of 154 psig. The temperature of the reactor was ramped up to 280°C at 1.5-2.0°C/min. After 15 hr at 280°C, the temperature was reduced to 265°C. When the temperature reached 265°C, the pressure was increased to 290 psig and the space velocity was increased to 2.4 nL/hr/g(Fe). These reaction conditions were maintained for the remainder of the run. Catalyst samples were taken periodically during the run as shown in Table VI.5.3.

RJO044 - The same pretreatment and synthesis conditions were used as for RJO043 except He (S.V.=1.0 nL/hr/g(Fe)) was passed over the catalyst during the ramping of the temperature from room temperature to 280°C. The He flow was continued for 1 hr after reaching 280°C and then synthesis gas was started (S.V.=2.0 nL/hr/g(Fe)). Catalyst samples were taken at the times indicated in Table VI.5.4.

Run RJO-139. 72.7 g of catalyst and 290 g of Drakeol-10 oil (Air Products) were loaded into a 1 liter stirred autoclave (operated at 900 rpm). The catalyst was pretreated with CO at 270°C, 175 psig and 2.0 nL/hr/g(Fe) for 24 hr. After pretreatment, H_2 flow was started to give a total space velocity of 3.4 nL/hr/g(Fe) and a composition of $H_2/CO=0.7$. Mass flow regulators were used to control the CO and H_2 flow rates. The temperature and pressure were maintained at 270°C (±2°) and 175 psig, respectively throughout the run.

The reactor effluent passed through a heated transfer line to a trap maintained at 60°C and then to a cold trap maintained at ~0°C. A third trap, maintained at

200°C, was occasionally utilized for collecting reactor wax. This reactor wax trap was connected by a transfer line to a filter in the reactor which removed catalyst particles from the wax. The effluent from the cold trap was passed to on-line GC's for analysis of the exit stream. A Carl-Hach gas analyzer was used to quantify CO, H_2, CO_2, ethane, ethene, propane, propene, butanes and butenes. A GC equipped with a Porpack Q column was utilized to quantify C_4 through C_9 hydrocarbons. Samples obtained from the three traps were mixed according to the amount produced during each mass balance period and were analyzed by capillary GC. The reactor was also equipped with a dip-tube which permitted catalyst slurry samples to be withdrawn periodically at the times indicated in Table VI.5.5.

RJO-140. A 20 wt. % slurry of catalyst and oil were added to a 1 liter stirred autoclave as described above. He was passed through the reactor at a flow rate of 300 cc/min. The reactor was pressurized to 150 psig and stirred at 900 rpm. The temperature of the reactor was ramped to 200° C at 2.0°C/min. Synthesis gas flow was started (H_2/CO=0.7) at a space velocity of 2.0 nL/hr/g(Fe) and 150 psig. The temperature was increased to 280°C at a rate of 7°C/hr. The temperature was maintained at 280°C for 12 hr and then the pressure was increased to 200 psig, the space velocity was increased to 2.5 nL/hr/g(Fe) and the temperature was decreased to 265°C. These conditions were maintained for the remainder of the run. Analyses of the reactor effluent and products were carried out as described above. Catalyst samples were withdrawn at the times indicated in Table VI.5.6.

In other runs performed on this catalyst, it was found that there was a difference in the activity of the catalyst when it was pretreated with 100% CO and

when an internal standard of N_2 was added to the CO. Runs RJO-143 and RJO-144 were carried out to see if there were structural differences in the catalysts following pretreatment.

RJO-143. 35.0 g of catalyst and 140 g of C_{30} polyalphaolefin oil (Ethylflo) were added to a 300 cc stirred autoclave. The reactor was stirred at 750 rpm, pressurized to 175 psig with a CO flow of 2.0 nL/hr/g(Fe). The temperature was increased at a rate of 1.5-2.0°C/min to 270°C. These conditions were maintained for 24 hr. The reactor effluent was periodically trapped in a sample bomb and analyzed by GC for CO and CO_2 content. In addition, catalyst samples were withdrawn from the reactor and analyzed by XRD and BET.

RJO-144. The same conditions were utilized as described for RJO-143 except that the gas composition was 75% CO and 25 % N_2.

VI.5.2.a. Catalyst Analysis

Catalyst slurry samples were all soxhlet extracted using boiling toluene as solvent.

Mössbauer spectra of the catalyst samples were obtained from a constant acceleration spectrometer with a γ-ray source consisting of 50-100 mCi of ^{57}Co in a Pd matrix. Spectra were analyzed using a least-squares fitting routine with the iron content of each phase determine from their relative peak areas.

Powder X-ray diffraction patterns of the catalysts were obtained using a Philips APD X-ray diffraction spectrometer equipped with a Cu anode and Ni filter operated at 40 kV and 20 mA ($CuK\alpha$=1.5418 Å). Iron phases were identified by comparing diffraction patterns of the catalyst samples with those in the standard powder X-ray

diffraction file compiled by the joint committee on powder diffraction standards published by the International Center for Diffraction Data.

Nitrogen sorption measurements were made with a Quantachrome Autosorb 6 instrument. Samples were outgassed at 80°C and less than 50 mtorr for a minimum of 12 hr prior to analysis. BET surface areas and pore size distributions were calculated from the adsorption and desorption data, respectively.

VI.5.3. RESULTS AND DISCUSSION

VI.5.3.a. UCI L-3950

RJO-043 and RJO-044. The activity of the catalyst was slightly lower during the activation period when heated to 200°C under He; however, the activity for the two runs was identical at the start of the synthesis conditions (Figures VI.5.1 and VI.5.2). The catalyst was not stable during either of the runs; synthesis gas conversion decreased from a high of 58% to >40% after 72 hr on stream. The catalyst slurry samples were very thick and viscous after 48 hr of synthesis; repeated extractions with toluene and o-xylene could not remove all of the heavy wax as shown by XRD. The heavy wax production is consistent with the high level of potassium present in the catalyst and may have rendered the catalyst slurry too viscous to obtain adequate gas distribution thereby lowering the synthesis gas conversion. There appears to be no major difference in the activity of the catalyst when activated in synthesis gas or in He followed by synthesis gas.

Catalyst Characterization. The Mössbauer spectrum of the fresh, calcined catalyst taken at 10 K is shown in Figure VI.5.3. Three magnetically split components comprising 97% of the spectral area and a superparamagnetic component (3%) were

required for a good fit of the data. The sextet with the largest hyperfine field was assigned to α-Fe_2O_3 . The other two sextets were assigned to some ferric oxide resulting from the substitution of Si^{4+} or Cu^{2+} cations or vacancies in the crystal lattice of α-Fe_2O_3. The superparamagnetic component is assigned to a ferric oxide, perhaps very small α-Fe_2O_3 particles.

XRD of the catalyst after heating to 265°C under $CO+H_2$ (2.0 nL/hr/g(Fe)) at 154 psig showed only α-Fe_2O_3. Seven hours after reaching the activation temperature of 280°C, XRD showed, in addition to α-Fe_2O_3, Fe_3O_4 and χ-Fe_5C_2. Following an additional 8 hr at activation conditions and 2 hr at synthesis conditions, the α-Fe_2O_3 phase decreased, the Fe_3O_4 phase remained constant and the χ-Fe_5C_2 phase increased. After 24 hr at synthesis conditions, a new phase appeared in addition to the three mentioned above. This phase was assigned as the potassium iron(II,III) hydroxide silicate, ferriannite ($KFe_3(FeSi_3)O_{10}(OH)_2$). By the end of the run, the ferriannite phase had increased considerably (Figure VI.5.4), and a small amount of ϵ'-$Fe_{2.2}C$ could be detected in addition to Fe_3O_4 and χ-Fe_5C_2. No α-Fe_2O_3 could be detected. Mössbauer spectroscopy results are shown in Figure VI.5.5. The room temperature Mössbauer spectrum of the catalyst withdrawn at 130°C during the heat up to activation conditions shows 6% magnetically split α-Fe_2O_3 and 94% superparamagnetic ferric oxide. The spectrum taken at 10 K is more complex, closely resembling that of the fresh calcined catalyst. The spectrum consists of 36% α-Fe_2O_3 and the remainder, some ferric oxide(s) resulting from substitution and/or vacancies in the α-Fe_2O_3 lattice. The spectrum of the catalyst taken seven hr after reaching activation conditions shows substantial conversion to χ-Fe_5C_2 (22%) and Fe_3O_4 (10%).

A small component (8%) of magnetically split α-Fe_2O_3 was present while the largest fraction (60%) belonged to a superparamagnetic component assigned to a ferric oxide. Two hr after changing to synthesis conditions, the χ-Fe_5C_2 fraction was 26% while the Fe_3O_4 fraction had grown to 18%. No magnetically split α-Fe_2O_3 could be detected in this sample; however, a large amount (56%) of the superparamagnetic component was still present. This superparamagnetic component could be small particle iron carbide and/or iron oxide. A new phase comprising 6% of the spectrum could be detected after 24.5 hr at synthesis conditions which was assigned as an iron silicate. The major phases at this time were χ-Fe_5C_2 (49%), superparamagnetic component (31%) and Fe_3O_4 (14%). After 49.5 hr at synthesis conditions the iron silicate phase had grown to 13% while the other phases had remained essentially unchanged. By the end of the run, 96 hr at synthesis conditions, the Fe_3O_4 phase had shrunk to 7% and the iron silicate phase had grown to 27%. χ-Fe_5C_2 was still the major phase (37%) and the superparamagnetic component was present at 29%.

Different results were obtained when the catalyst was brought up to activation temperature (280°C) under He. After heating to 130°C at 154 psig, only α-Fe_2O_3 was present. Six hr after switching to $CO+H_2$, the catalyst had partially reduced to Fe_3O_4 and a mixture of ϵ'-$Fe_{2.2}C$ and χ-Fe_5C_2; however, the dominant phase was still α-Fe_2O_3. Two hr after switching to synthesis conditions, no α-Fe_2O_3 could be detected and the amount of ϵ'-$Fe_{2.2}C$ had increased dramatically while only a small amount of χ-Fe_5C_2 was present. As the run progressed the dominant phases appeared to be Fe_3O_4 and ϵ'-$Fe_{2.2}C$ with a very small amount of χ-Fe_5C_2. By the end of the run a small amount of ferriannite may also have been present. Mössbauer results of RJO-044 are shown in Figure VI.5.6. Mössbauer of the sample withdrawn after heating to

130°C under He was similar to that of the sample heated up under $CO+H_2$. Magnetically split α-Fe_2O_3 was present at 11% while the remainder was superparamagnetic ferric oxide. Six hr after starting the synthesis gas during the activation period, the catalyst showed partial reduction to carbides and Fe_3O_4 (20%). The carbide phases present were ϵ'-$Fe_{2.2}C$ (15%) and χ-Fe_5C_2 (6%). The remainder (59%) of the catalyst was a superparamagnetic component. Two hr after reaching synthesis conditions the ϵ'-$Fe_{2.2}C$ phase had swelled to 44% while the χ-Fe_5C_2 phase was present as 19%. The remainder of the catalyst was Fe_3O_4 (12%) and superparamagnetic material (25%). After 49.5 hr at synthesis conditions, little change in the catalyst composition had occurred. By the end of the run at 96 hr, the Fe_3O_4 phase had grown to 30% at the expense of the superparamagnetic phase which decreased to 22%. χ-Fe_5C_2 and ϵ'-$Fe_{2.2}C$ were both present at 10% and 38% respectively.

VI.5.3.b. UCI 1185-57

RJO-139 and RJO-140. The activity and stability of the catalyst was much better when activated in CO than in synthesis gas. Total $CO+H_2$ conversions for the CO activated catalyst started at about 68%, rose to 78% after 65 hr and then steadily decreased to 65% at the end of the run (140 hr). The catalyst activated in synthesis gas showed low conversion (<5%) during the first 8 hr of activation. After 10 hr of activation the conversion rose to 18% and eventually peaked at 59% after 14 hr. By the end of the activation period, the total conversion was 58%; however, switching to synthesis conditions caused a rapid decline in the conversions to about 30% (Figure VI.5.7). The rapid drop in activity was most likely caused by decreasing the

temperature from 280°C to 265°C. The temperature of the reactor dropped to 200°C after 50 hr at synthesis conditions indicating that the catalyst had deactivated. Upon opening the reactor it was found that the autoclave had become dry. Apparently the start-up oil was too light and evaporated during the run; the activity of the catalyst was too low to replace the lost oil and the catalyst deactivated. The slow decline of the activity of the catalyst pretreated in CO may also have been due to boiling off the start-up oil. Additional runs utilizing a heavier wax as the start up fluid have shown stable conversions in excess of 80% when the catalyst is pretreated with CO.

The alkene selectivity for the C_2-C_4 fractions are shown in Figure VI.5.8 for the CO activated catalyst and in Figure VI.5.9 for the syn-gas activated catalyst. In general the amount of alkene decreases for both runs as the conversion increases and increases when the conversion decreases. During maximum conversion the C_2, C_3 and C_4 alkene selectivities were 25%, 75% and 83%, respectively for the CO activated catalyst. These values are very similar to those of the syn-gas activated catalyst during activation; however, during the synthesis stage of the run, when the conversion dropped to <30%, the C_2, C_3 and C_4 olefin selectivities increased to >60%, and >80% and 88%, respectively. The fraction of 1-alkene as compared to 1-alkene+2-alkene for the C_4 fraction is shown for the two runs in Figure VI.5.10. At the start of the runs, when the conversions were low, the olefin fraction was at least 80% 1-alkene. At the peak conversion this dropped to below 45%. As the catalysts deactivated, the 1-alkene content rose. Presumably at high $CO+H_2$ conversions, the vapor pressure of CO and H_2 decrease and more sites for adsorption of olefins

become available. This leads to an increase in secondary reactions such as olefin hydrogenation and isomerization.

The Fischer-Tropsch reaction over iron catalysts can be expressed as the following equations:

$$CO + 2H_2 \rightarrow -CH_2- + H_2O \qquad \text{(VI.5.1)}$$

$$CO + H_2O \rightarrow H_2 + CO_2 \qquad \text{(VI.5.2)}$$

which when combined, give

$$2CO + H_2 \rightarrow -CH_2- + CO_2 \qquad \text{(VI.5.3)}$$

Equation 1, the hydrogenation of CO, occurs readily on Co and Ni catalysts. Equation 2, the water-gas shift reaction (WGS) proceeds to equilibrium on iron catalysts operating above 50% conversion. The ability of iron catalysts to convert water to H_2 enables synthesis gas lean in hydrogen to be used in the FT synthesis. This is important since modern coal gasifiers produce syn-gas with H_2/CO ratios of about 0.5 to 0.7. An easy measure of the WGS activity of an FT catalyst can be determined by relating the amount of CO converted to the amount of CO_2 produced; equation 3 shows that CO_2/CO ratio should be 0.5 for complete WGS. The CO_2/CO ratio of the catalyst pretreated in CO remained approximately 0.5 throughout the run. The reaction quotient, $K_{app}=P_{CO2}P_{H2}/(P_{CO}P_{H2O})$, is approximately 62 for the WGS at equilibrium under the run conditions for RJO-139; however, data for this run indicate that K_{app} did not exceed 50% of the equilibrium value. The catalyst activated in synthesis gas had a lower WGS activity as indicated by a CO_2/CO ratio of about 0.48. The lower WGS activity is related to the lower overall activity of RJO-140.

Hydrocarbon production rates for RJO-139 are shown in Figure VI.5.11. The product distribution in terms of an Anderson-Shulz-Flory plot is shown in Figure VI.5.12. The plot is typical of the product distribution for iron based FT catalysts; two distinct slopes could be detected. This distribution was modeled according to the procedure outlined by Satterfield with α_1=0.68, α_2=0.88 and the carbon number of the break point equal to 12.9 (VI.5.6).

Mössbauer spectroscopy and XRD both clearly indicate that the catalyst is completely converted to a mixture of iron carbides during CO pretreatment (Table VI.5.5). The carbides identified by XRD are χ-Fe_5C_2 and ϵ'-$Fe_{2.2}C$. The iron composition after CO pretreatment, according to Mössbauer spectroscopy, is 90% χ-Fe_5C_2 and 10% some superparamagnetic phase which could be a carbide or oxide. The isomer shift and quadrupole moment of the superparamagnetic doublet indicate the presence of small particle ϵ'-$Fe_{2.2}C$. Figure VI.5.13 shows the phase transformation of the catalyst during the pretreatment and synthesis; in general, the catalyst is partially oxidized to Fe_3O_4 during the first 140 hr of synthesis. This is most likely due to an accumulation of H_2O and CO_2 in the reactor. Results of the Mössbauer and XRD analyses for the catalyst activated in synthesis gas are shown in Table VI.5.6 and Figure VI.5.14. XRD and Mössbauer spectroscopy both show that the only iron phase present after heating to 200°C under He was α-Fe_2O_3. XRD shows the catalyst was rapidly converted to Fe_3O_4 during the first 3.5 hr of activation. Mössbauer analysis shows the only iron phase present after 7 hr of activation was Fe_3O_4; however, XRD identified a small amount of iron carbide. After 11.25 hr of activation, 5% of the iron was present as ϵ'-$Fe_{2.2}C$ and 5% as a superparamagnetic

phase with the remaining 90% present as Fe_3O_4. The carbide content of the catalyst grew to 35% of the total iron at the end of the pretreatment (23% ϵ'-$Fe_{2.2}C$ and 12% χ-Fe_5C_2) and the superparamagnetic component grew to 16%. The catalyst continued to carbide during the synthesis stage of the run; the iron composition was 17% Fe_3O_4 and 77% iron carbides with the remainder a superparamagnetic phase after 50 hr of synthesis.

It is difficult to correlate the phase composition of the 1185-57 catalyst with the differences in activity when the catalyst is pretreated in CO or synthesis gas. The CO pretreatment converted 90% of the iron in the catalyst to χ-Fe_5C_2 while synthesis gas activation converted 35% of the iron to a mixture of χ-Fe_5C_2 and ϵ'-$Fe_{2.2}C$. Activity during the synthesis gas activation was relatively high so it is unlikely that the difference in activity is due to the amount of iron carbide or Fe_3O_4 present. It is apparent that the lower activity of the synthesis gas activated catalyst is due to a lower surface area of the catalyst. The catalyst had a surface area of 83 m^2/g after 140 hr of synthesis when activated in CO as compared to 12 m^2/g after 50 hr of synthesis when activated in synthesis gas. Another possibility for the low activity of the catalyst when activated in synthesis gas is that it produced a product too light to replace volatilized start-up oil; the reactor was essentially dry at the end of the run. As the oil evaporated the catalyst slurry would have become too viscous to obtain good mixing of the synthesis gas with the catalyst.

RJO-143 and RJO-144. The BET surface area and pore volume of the UCI 1185-57 catalyst at various time of reduction in CO are shown in Figure VI.5.15. The catalyst as received had a relatively low surface area of only 13 m^2/g. The surface area and pore volume were found to oscillate during the first 8 hr of CO exposure and

then increased to 18 m^2/g and 35 m^2/g after 26.5 hr of CO treatment. XRD analysis shows that the phases present for both runs were identical. The catalyst was initially converted to Fe_3O_4 during the first 2.5 hr of CO treatment and then gradually carbided to χ-Fe_5C_2 and ϵ'-$Fe_{2.2}C$. No Fe_3O_4 could be seen in the XRD diffractograms of the catalyst at the end of the CO treatment. These XRD results very similar to those obtained for RJO-139.

Plots of CO_2 concentration in the exit stream and cumulative CO_2 moles produced during the CO reduction of the UCI 1185-57 catalyst are shown in Figures VI.5.16 and VI.5.17. A peak in the CO_2 production occurs after approximately 2.5 hours of exposure to CO during the heat-up from 25°C to 270°C. This peak probably is due to the rapid reduction of α-Fe_2O_3 to Fe_3O_4 and to a lesser extent the reduction of CuO to Cu metal or Cu_2O. Two additional peaks or shoulders are also seen in Figure VI.5.16; these may correspond to catalyst transformation to χ-Fe_5C_2 and ϵ'-$Fe_{2.2}C$ and/or to the formation of Boudouard carbon.

$$3Fe_2O_3 + CO \rightarrow 2Fe_3O_4 + CO_2 \qquad \text{(VI.5.4)}$$

$$5Fe_3O_4 + 32CO \rightarrow 3Fe_5C_2 + 26CO_2 \qquad \text{(VI.5.5)}$$

$$2CuO + CO \rightarrow Cu_2O + CO_2 \qquad \text{(VI.5.6)}$$

$$Cu_2O + CO \rightarrow 2Cu + CO_2 \qquad \text{(VI.5.7)}$$

$$2CO \rightarrow C + CO_2 \qquad \text{(VI.5.8)}$$

The theoretical amount of CO_2 produced during the reduction of a known amount of catalyst to χ-Fe_5C_2 and Cu metal can be calculated based on the above equations. Figure VI.5.17 shows the cumulative moles of CO_2 produced for Runs RJO-143 and RJO-144. Reduction with 100% CO produced more CO_2 and at a higher rate than

reduction with a mixture of 75% CO and 25% N_2. The theoretical amount of CO_2 needed for complete reduction of the catalyst was produced after about 8 hr for the RJO-143 (100% CO) and after about 19 hr for RJO-144 (75% CO/25% N_2). Treatment with CO for 26.5 hr produced approximately 49% and 8% more CO_2 than necessary for complete reduction of the catalyst for RJO-143 and RJO-144, respectively. The excess CO_2 production implies that Boudouard carbon was deposited on the catalyst in both runs. Elemental analyses showed the catalysts were composed of 21% and 18% carbon, for RJO-143 and RJO-144, respectively. This is compared to 7.9% carbon for pure χ-Fe_5C_2. Carbon deposition is also substantiated by the increase in the BET surface area of the catalysts during the CO treatment; this has been correlated with an increase in elemental carbon (VI.5.6). XRD results indicate that the catalyst in RJO-143 was completely reduced to χ-Fe_5C_2 and ϵ'-$Fe_{2.2}C$ between 15.5 hr and 20.5 hr of CO exposure and RJO-144 was reduced completely to iron carbides between 20.5 hr and 23.5 hr of CO exposure. The catalyst was reduced to χ-Fe_5C_2 and ϵ'-$Fe_{2.2}C$ at least 7 and 1.5 hr after the stoichiometric amount of CO_2 had been produced for RJO-143 and RJO-144, respectively. This implies that reduction to iron carbide(s) does not precede the deposition of Boudouard carbon, but that they occur simultaneously.

Wiltowski et al. have studied the kinetics and mechanism of reduction of iron sulfide with CO (VI.5.7). The type of reaction rate equation which describes the reduction was determined by the method of Gardner. The slope of the line determined by plotting ln[-ln(1-α)] as a function of ln(t), where α is the degree of reduction and t is the time of reduction, determines the type of rate equation which

governs the process. Similar plots for the reduction of UCI 1185-57 in CO are shown in Figure VI.5.18. The plots for RJO-143 and RJO-144 are reasonably linear with correlations above 0.98 and slopes of 1.79 and 1.37 respectively. The slopes do not correlate with any of the reaction rate equations listed by Wiltowski et al.; this supports the contention that the reduction of the catalyst by CO involves more than one reaction mechanism.

It is apparent that pretreatment of the UCI 1185-57 catalyst for 26.5 hr with a mixture of 75% CO and 25% N_2 produces less Boudouard carbon and a higher BET surface area than when pretreated with 100% CO. The lower activity found when pretreating the catalyst with 100% CO as compared to 75% CO can be explained in terms of the active sites being covered by a layer of graphitic carbon.

VI.5.4. REFERENCES

VI.5.1. Rao, V. U. S., Stiegel, G. J., Cinquegrane, G. J., and Srivastava, R. D., *Fuel Processing Technology*, **30**, 83 (1992).

VI.5.2. Kölbel, H., and Ralek M., *Catal. Rev.-Sci. Eng.*, **21**, 225 (1980).

VI.5.3. Bukur, D. B., Lang, X., Rossin, J. A., Zimmerman, W. H., Rosynek, M. P., Yeh, E, B., and Li, C., *Ind. Eng. Chem. Res.*, **28**, 1130 (1989).

VI.5.4. Huang, C.-S., Xu, L., and Davis, B. H., *Fuel Sci. & Technol. Int.*, **11**, 639, (1993).

VI.5.5. Huang, C.-S., Ganguly, B., Huffman, G. P., Huggins, F. E., and Davis B. H., *Fuel Sci. & Technol. Int.*, **11**, 1289 (1993).

VI.5.6. Donnelly, T. J., Yates, I. C., Satterfield, C. N., *Energy & Fuels*, **2**, 734 (1988).

VI.5.7. Vogler, G. L., Jiang, X.-Z., Dumesic, J. A., and Madon, R. J., *J. Catal.*, **89**, 116 (1984).

VI.5.8. Wiltowski, T., Hinckley, C. C., Smith, G. V., Nishizawa, T., Saporoschenko, M., Shiley, R. H., and Webster, J. R., *J. Solid State Chem.*, **71**, 95 (1987).

Table VI.5.1

Catalyst Composition in Wt.%

Catalyst	Fe_2O_3	K_2O	CuO	SiO_2	Kaolin
L-3950	80.2	2.84	3.51	13.5	
1185-57	62.3	0.93	5.58		31.2

Table VI.5.2

Run Conditions

Run	Catalyst	Pretreat	Solvent	Temperature	Pressure	S.V.
RJO-043	L-3950	1	C-30	265	290	2.4
RJO-044	L-3950	2	C-30	265	290	2.4
RJO-139	1185-57	3	Drakeol	270	175	3.4
RJO-140	1185-87	4	Drakeol	265	200	2.5
RJO-143	1185-87	5	C-30			
RJO-144	1185-87	6	C-30			

Pretreat 1: 280°C, 154 psig H_2/CO = 0.7; 2.0 nL/hr/g(Fe); heat to 280°C at 2.0°C/min. and hold for 24 hr.; stirrer speed 750 rpm.

Pretreat 2: 280°C, 154 psig H_2/CO = 0.7; 2.0 nL/hr/g(Fe); heat to 280°C at 2.0°C/min. under He. After reaching 280°C, switched to CO + H_2 and held for 24 hrs.; stirrer speed 750 rpm.

Pretreat 3: 270°C; 175 psig CO; 2.0 nL/hr/g(Fe); heat to 270°C at 2°C/min. and held at 270°C for 24 hrs.; stirrer speed 900 rpm.

Pretreat 4: 280°C, 150 psig H_2/CO = 0.7; 2.0 nL/hr/g(Fe); heat to 200°C at 2.0°C/min. under He. After reaching 200°C, switched to CO + H_2 and heated to 280°C at 7°C/hr.; held conditions for 12 hrs.; stirrer speed 900 rpm.

Pretreat 5: 270°C; 175 psig CO (25% N_2); 2.0 nL/hr/g(Fe); heat to 270°C at 2°C/min. and held at 270°C for 24 hrs.; stirrer speed 750 rpm.

Table VI.5.3

RJO-043

Condition	Time, Hr.	Mössbauer Phase (% Fe)	XRD
As Received	N.A.	H(95), SO(5)	H
$CO + H_2$ ACtivation 265°C	3.5	SO(94), H(6)	H
280°C	13	SO(40), SC(22), χ(21) M(9), H(8)	H, M, $\chi\epsilon'$
Synthesis	2	SP(56), χ(26), M(18)	M, H, χ, ϵ'
	24.5	χ(49) SP(31), M(14), S(6)	χ, ϵ', M, F
	49.5	χ(47), SP(21), M(19), S(13)	M, χ, ϵ', F
	96	χ(37), SP(29), S(27), M(7)	χ, ϵ', M, F

SO = superparamagnetic oxide
SC = superparamagnetic carbide
SP = superparamagnetic component
M = Fe_3O_4
χ = Fe_5C_2
ϵ' = ϵ'-$Fe_{2.2}C$
S = iron silicate
F = $KFe_3(FeSi_3)O_{10}(OH)_2$

Table VI.5.4

RJO-044

Condition	Time, Hr.	Mössbauer Phase (% Fe)	XRD
As Received	N.A.	H(95), SO(5)	H
He, 265°C	3.5	SO(89), H(11)	H
$CO + H_2$ ACtivation 280°C	6	SO(59), M(20), ϵ'(15), χ(21)	H, M, $\chi\epsilon'$
Synthesis	2	ϵ'(44) SP(25), χ(19), M(12)	ϵ', M, χ
	24.5	SP(41), ϵ'(39), χ(11), M(9)	ϵ', M, χ
	49.5	ϵ'(45), SP(32), χ(13), M(10),	ϵ', M, χ
	96	ϵ'(38), SP(22), M(29), χ(11)	M, ϵ', χ

SO = superparamagnetic oxide
SP = superparamagnetic component
M = Fe_3O_4
χ = Fe_5C_2
ϵ' = ϵ'-$Fe_{2.2}C$
S = iron silicate
F = $KFe_3(FeSi_3)O_{10}(OH)_2$

Table VI.5.5

RJO-139

Condition	Time, Hr.	Surface Area, m^2/g	Pore Volume, cm^3/g	Mössbauer Phase (% Fe)	XRD
As Received	N.A.	13	0.066		H, K
CO Pretreatment	2.75			M(100)	M, K
	5.25			M(95), SC(5)	M, K, C
	9.25			M(62), χ(26), SC(12)	M, K, χ
	13.25			χ(56), M(33), SC(11)	K, M, χ, ϵ'
	21.25			χ(78), M(12),SC(10)	K, χ, M, ϵ'
	26.5	48	0.153	χ(90), SC(10)	K, χ, ϵ'
Synthesis	6			χ(87), SC(13)	K, χ, M, ϵ'
	19.75			χ(69), Sc(23), M(8)	χ, K, M, ϵ'
	27.75			χ(67), SC(23), M(10)	χ, K, M, ϵ'
	49			χ(62), SC(25), M(13)	χ, K, M, ϵ'
	140	83	0.306	χ(66), SC(18), M(16)	χ, K, M, ϵ'

M = Fe_3O_4
χ = Fe_5C_2
ϵ' = ϵ'-$Fe_{2.2}C$
C = iron carbide
K = kaolin

Table VI.5.6

RJO-140

Condition	Time, Hr.	Surface Area, m^2/g	Pore Volume, cm^3/g	Mössbauer Phase (% Fe)	XRD
As Received	N.A.	13	0.066		H, K
He, 200°C	12	24	0.101	H(94), SO(4)	H, K
CO + H_2 Activation	3.5				M, K
	7			M(100)	M, K, C
	9				M, K, C
	11.25	16	0.072	M(90), SC(5), ϵ'(5)	M, K, C
	15			M(74), SC(7), ϵ'(13), χ(6)	M, K, ϵ', χ
	23.75			M(49), ϵ'(23), SC(17), χ(12)	M, K, ϵ', χ
Synthesis	3.25	< 3	0.068	ϵ'(33), χ(27), M(25), SC(11)	ϵ', χ, M, K
	50.25	12	0.090	ϵ'(42), χ(35), M(17), SC(6)	ϵ', χ, M, K

SO = superparamagnetic oxide
SC = superparamagnetic carbide
M = Fe_3O_4
χ = Fe_5C_2
ϵ' = ϵ'-$Fe_{2.2}C$
C = iron carbide
K = kaolin

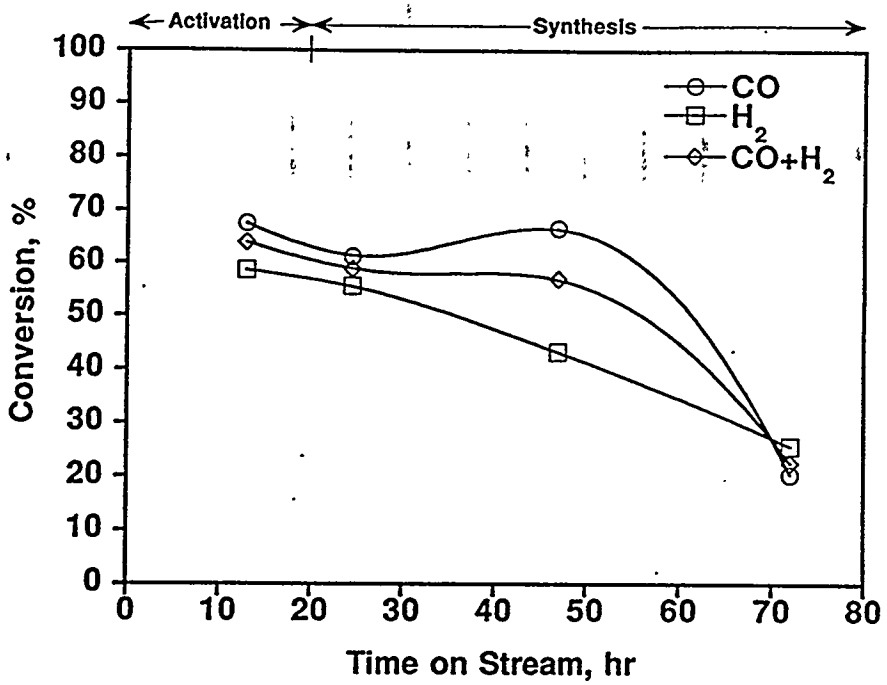

Figure VI.5.1. Synthesis gas conversion for RJO-043 as a function of time on stream.

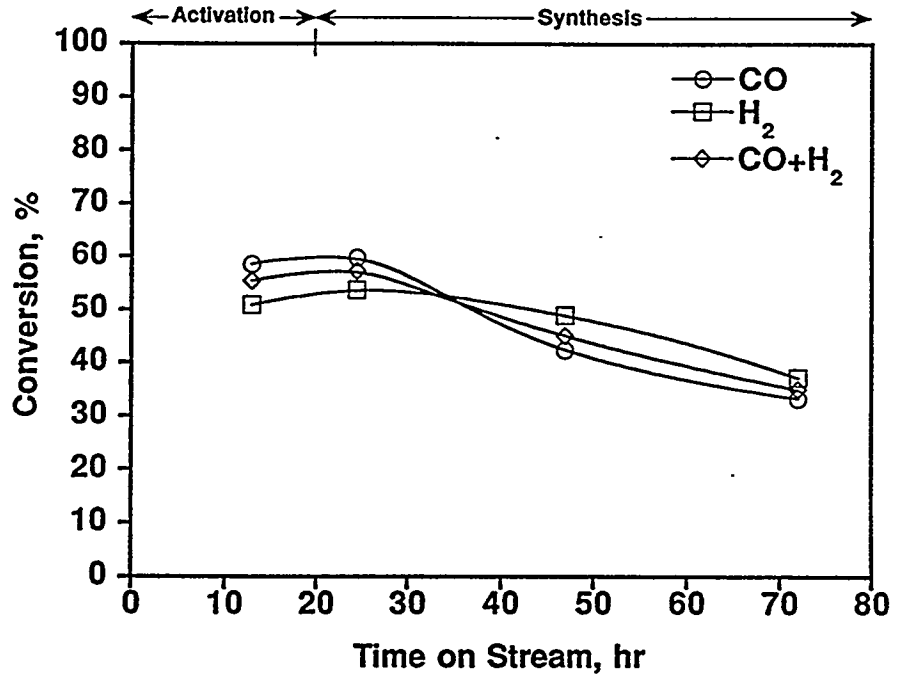

Figure VI.5.2. Synthesis gas conversion for RJO-044 as a function of time on stream.

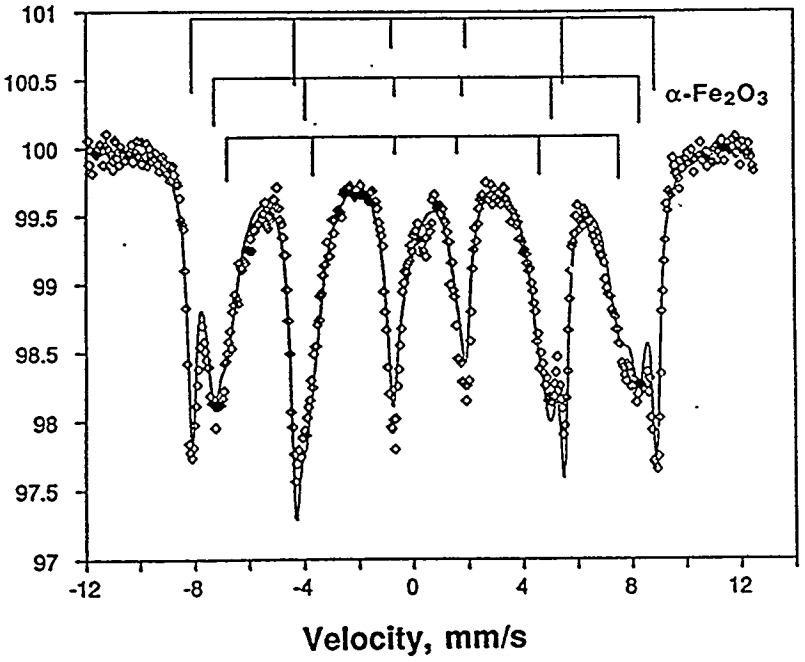

Figure VI.5.3. Mössbauer spectrum of as received L-3950 catalyst.

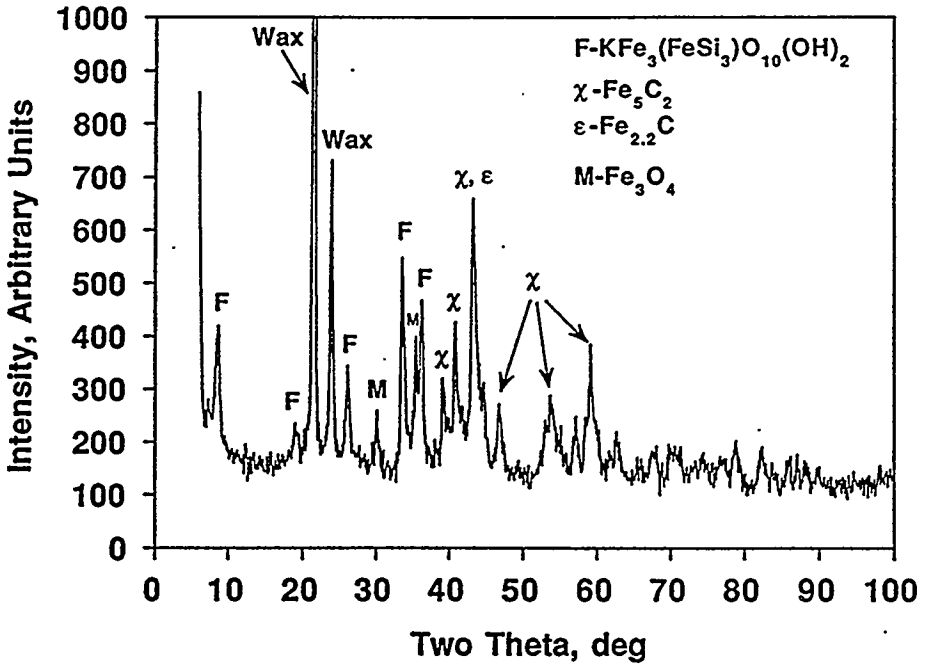

Figure VI.5.4. X-ray diffractogram of used catalyst from RJO-043.

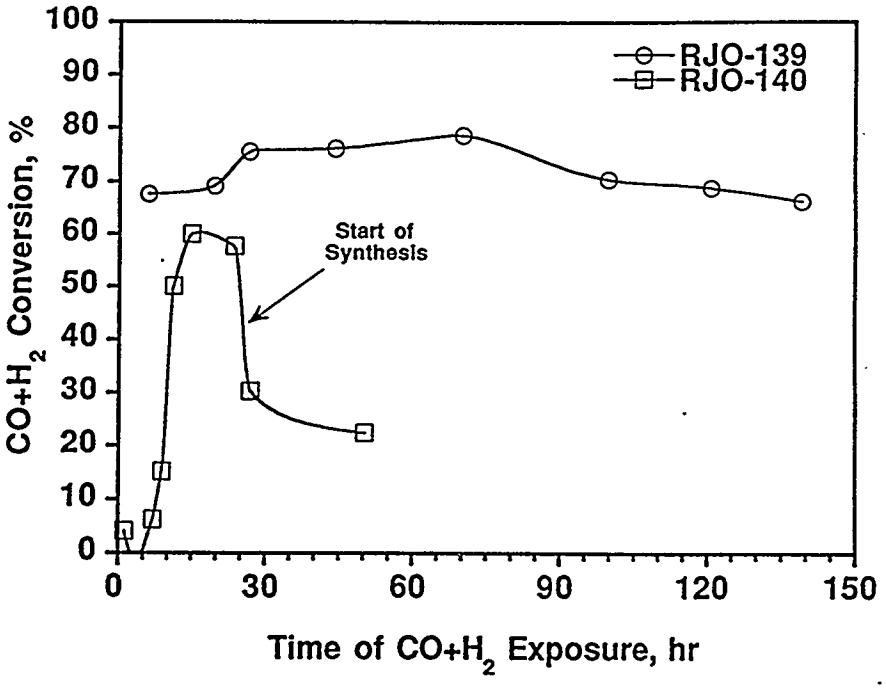

Figure VI.5.7. Synthesis gas conversion for RJO-139 and RJO-140 as a function of time on stream.

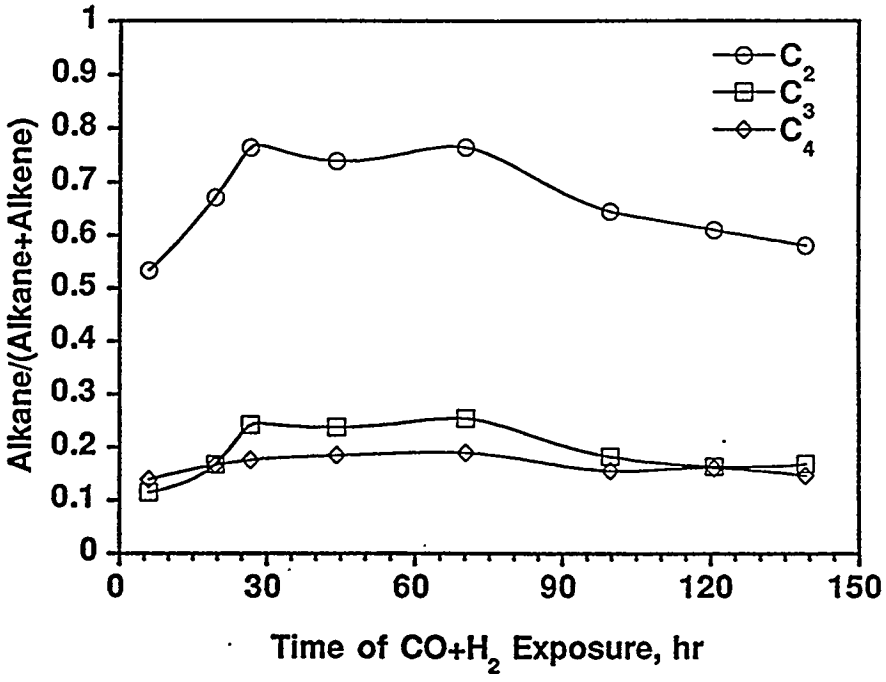

Figure VI.5.8. C_2, C_3, and C_4 alkane selectivity for RJO-139 as a function of time on stream.

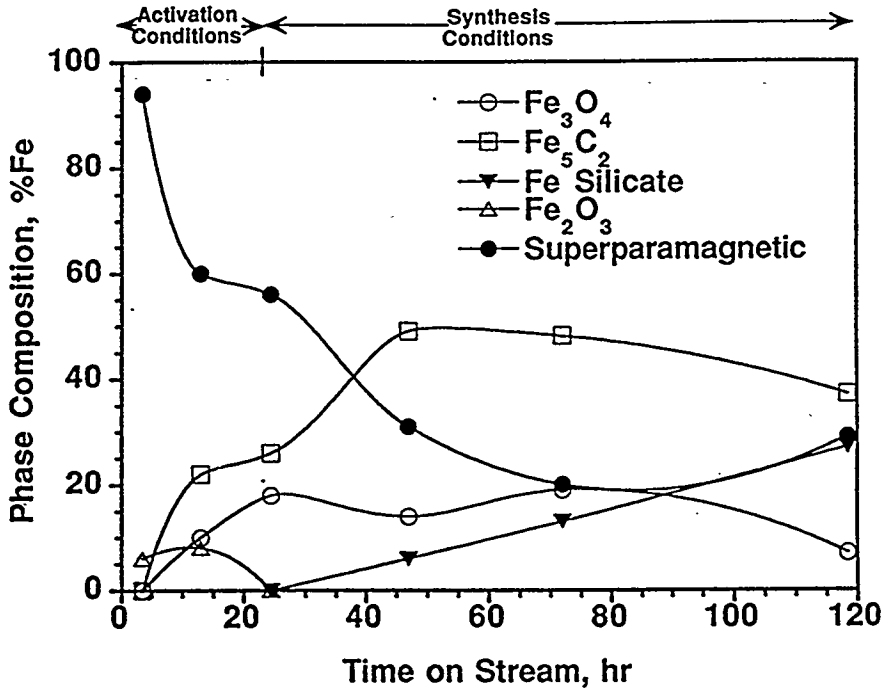

Figure VI.5.5. Mössbauer spectroscopy results for RJO-043 as a function of time on stream.

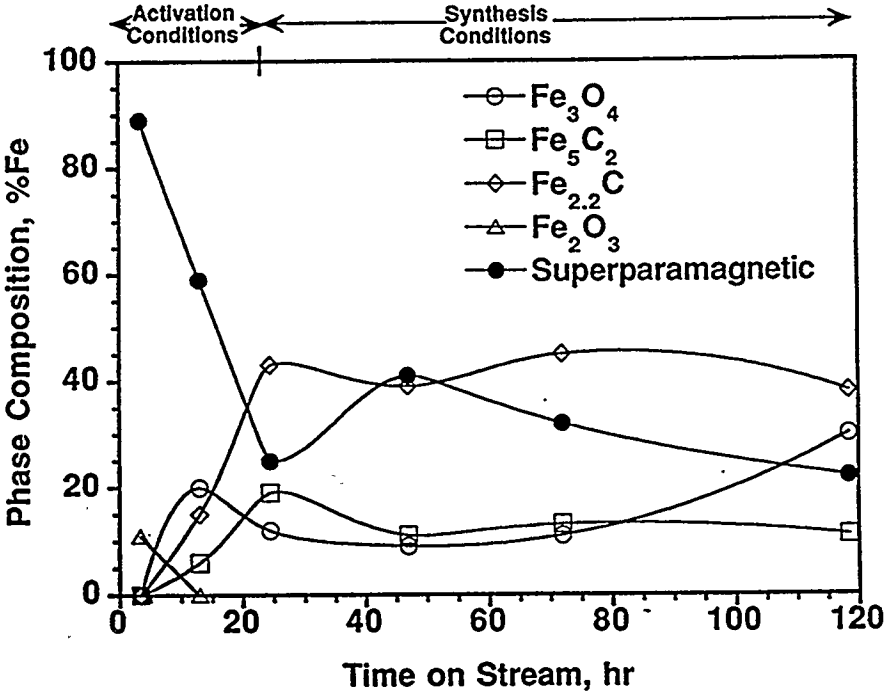

Figure VI.5.6. Mössbauer spectroscopy results for RJO-044 as a function of time on stream.

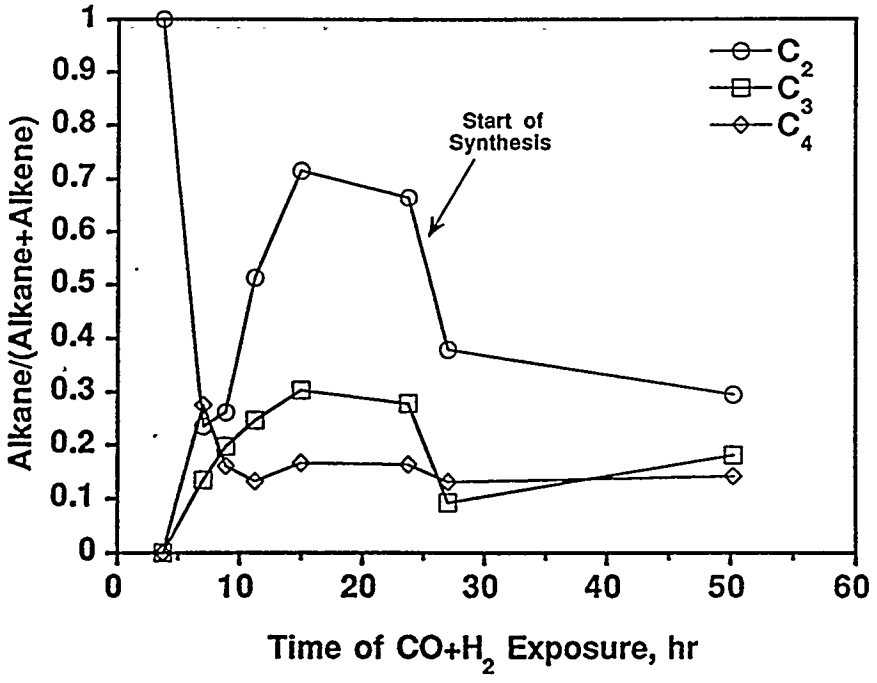

Figure VI.5.9. C_2, C_3, and C_4 alkane selectivity for RJO-140 as a function of time on stream.

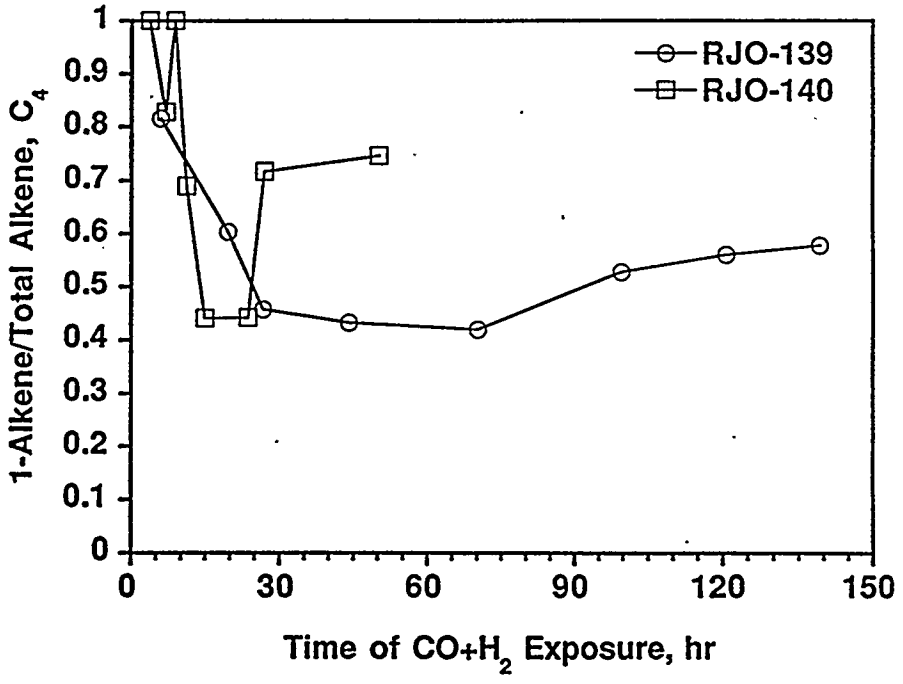

Figure VI.5.10. C_4 1-alkene selectivity for RJO-139 and RJO-140 as a function of time on stream.

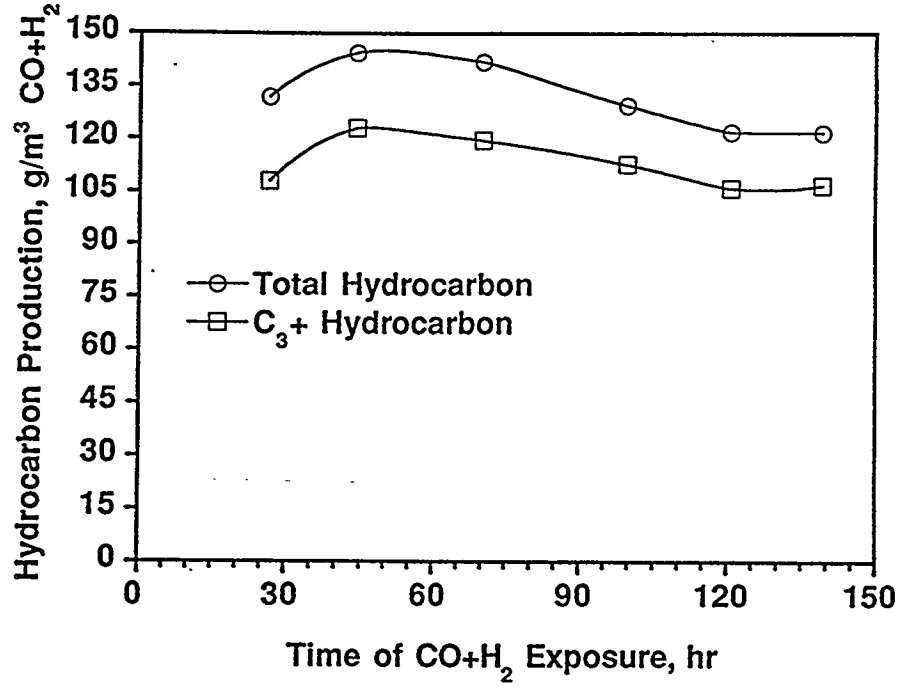

Figure VI.5.11. Hydrocarbon production as a function of time on stream for RJO-139.

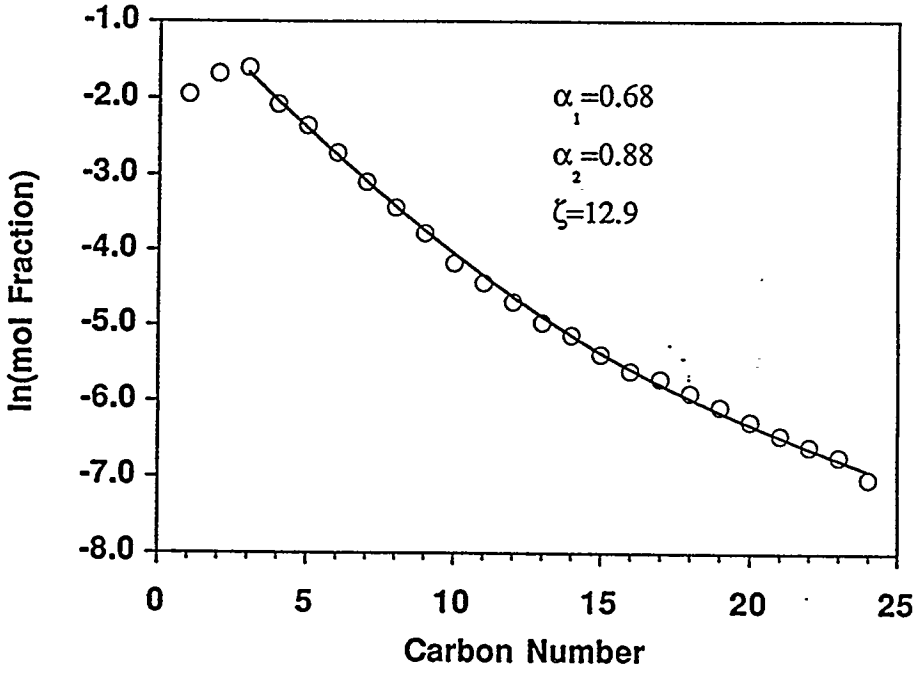

Figure VI.5.12. Anderson-Shulz-Flory plot for RJO-139.

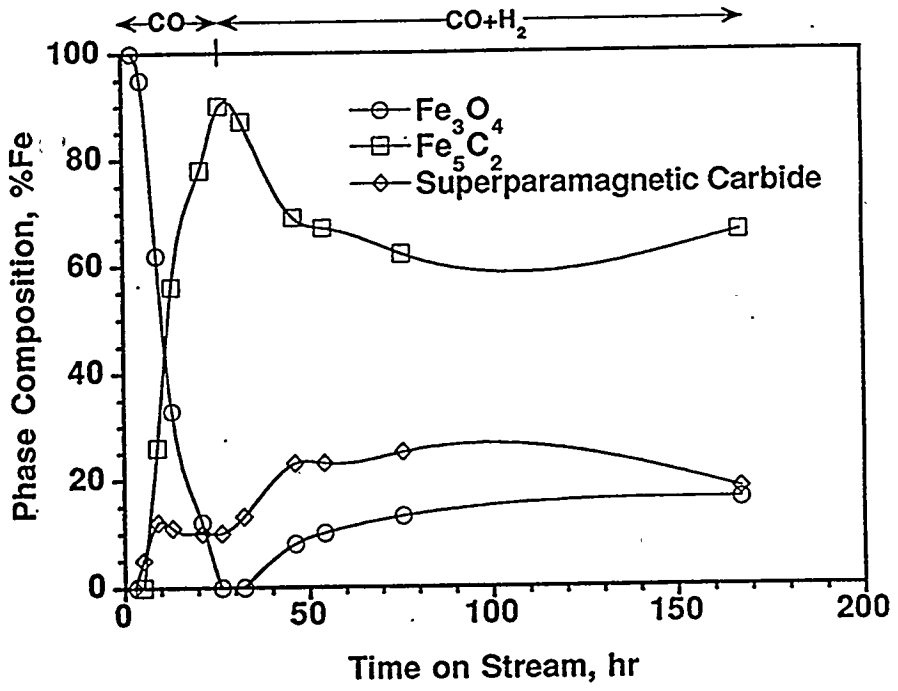

Figure VI.5.13. Mössbauer spectroscopy results for RJO-139 as a function of time on stream.

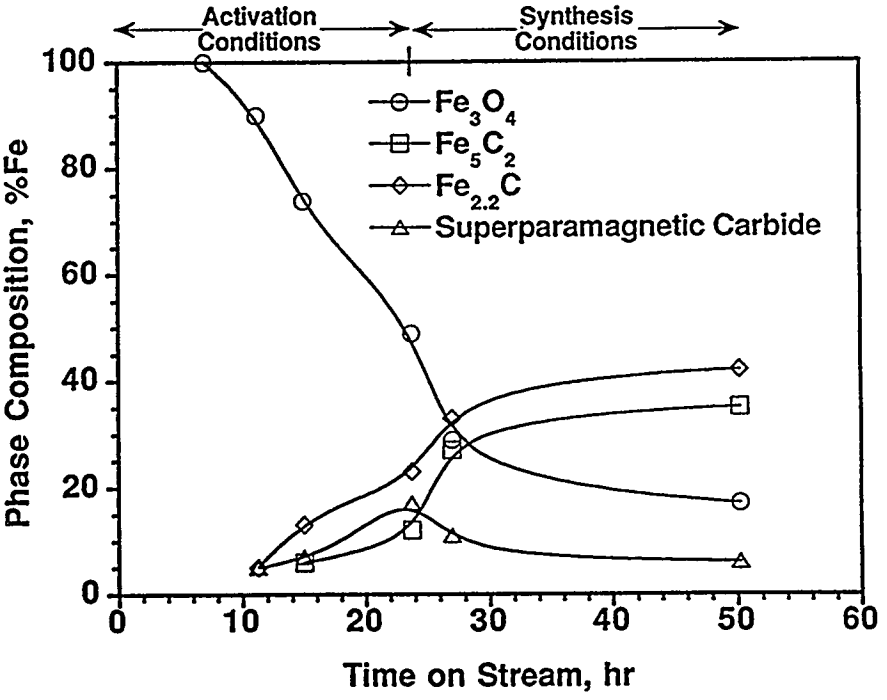

Figure VI.5.14. Mössbauer spectroscopy results for RJO-140 as a function of time on stream.

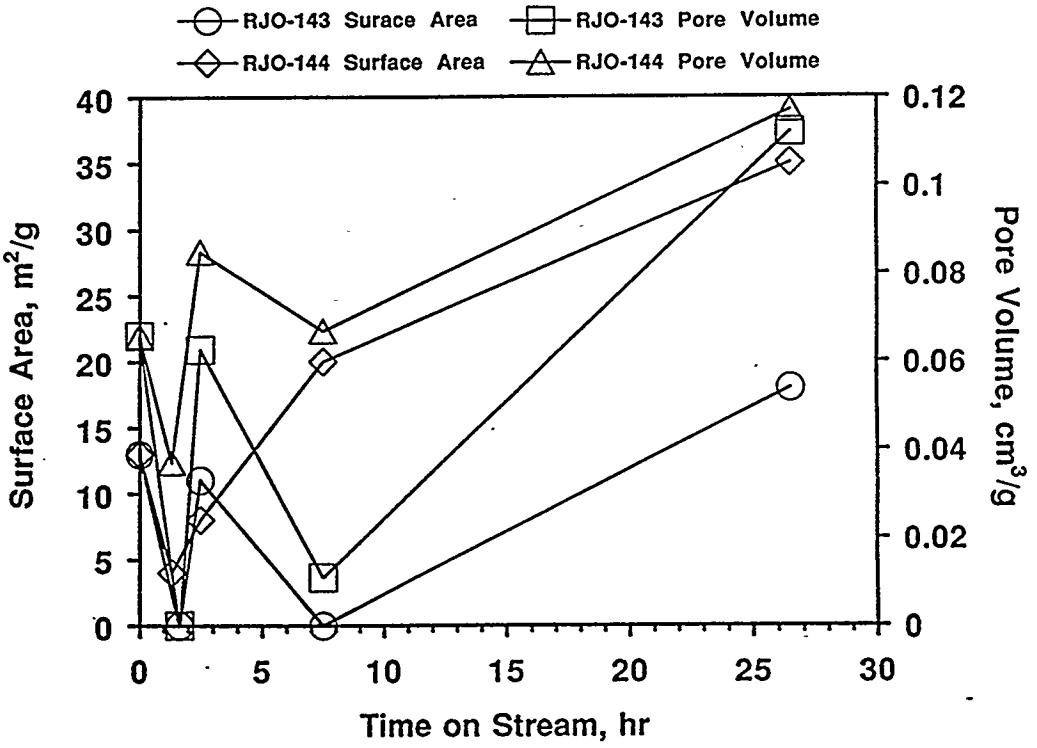

Figure VI.5.15. BET surface area and pore volume as a function of time on stream for RJO-143 and RJO-144.

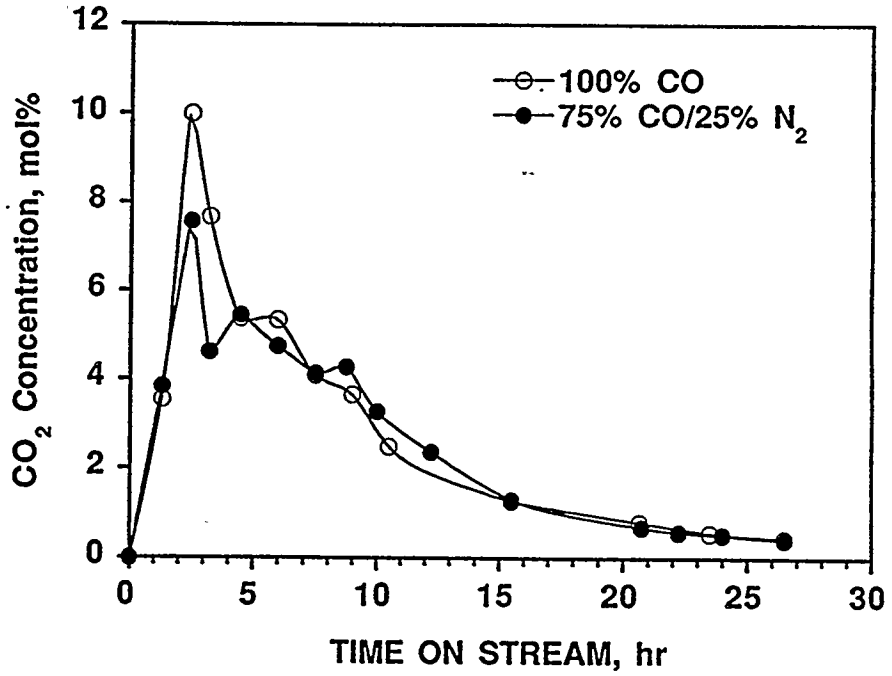

Figure VI.5.16. Concentration of CO_2 in the exit stream as a function of time on stream for RJO-143 and RJO-144.

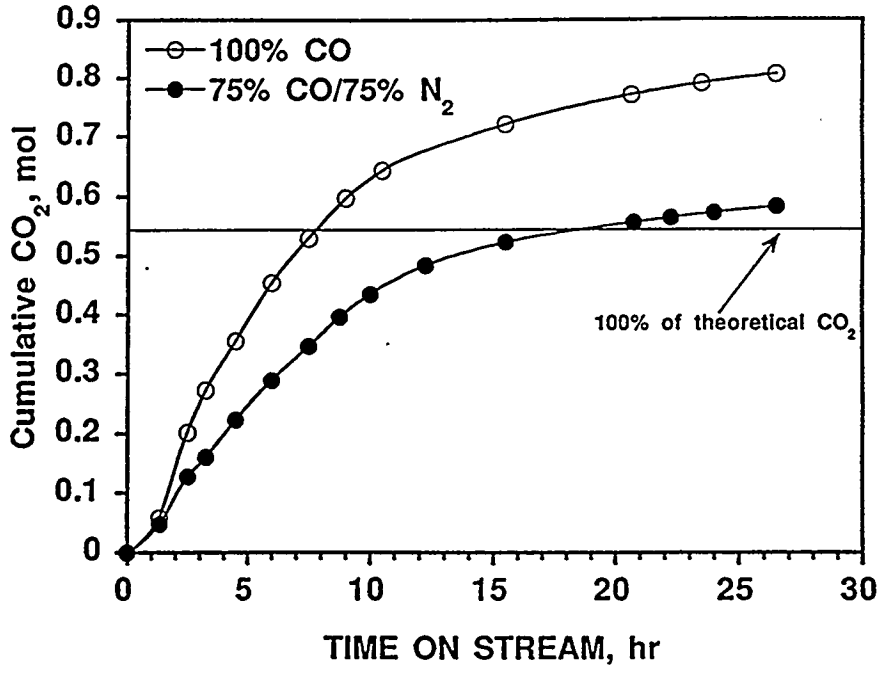

Figure VI.5.17. Cumulative CO_2 production as a function of time on stream for RJO-143 and RJO-144.

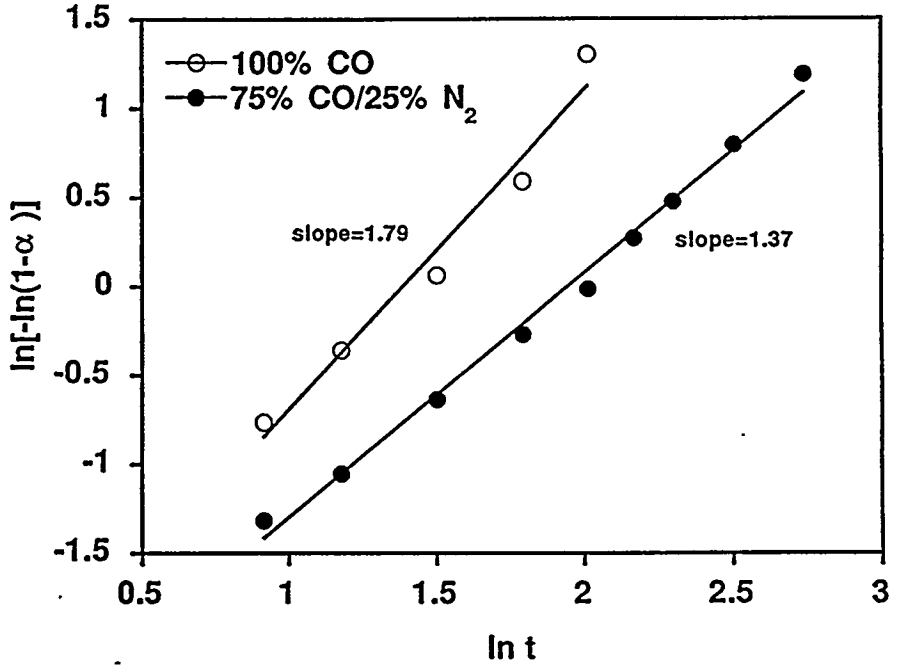

Figure VI.5.18. Plot of ln[-ln(1-α)] vs. ln(t) for RJO-143 and RJO-144, where α is the theoretical degree of catalyst reduction based on CO_2 production.